

Kyoji Sassa

---

## Abstract

A potential project of the International Programme on Landslides (IPL) was discussed among ICL members from Korea, China and Japan during one of the ICL meetings in Tokyo 2006. Based on these joint discussions, ICL headquarters in Japan, together with the Kyoto University (Disaster Prevention Research Institute) applied to the Japanese programme for Asian scientific cooperation for support to solve the common issues in the region, in cooperation with Japan, China, Korea, Indonesia, Philippines and Thailand. This Asian Joint Project was entitled “Development of early warning technology of landslides”. The application was accepted in 2007, and the project was approved as a part of IPL 105 in the same year. This chapter describes the early warning technologies developed in IPL 105 which are presented in published papers in the thematic issue of Early Warning of Landslides, Vol. 7, No. 3, 2010. Social implementation, capacity development, information dissemination and training for evacuation also have been implemented in this project; these activities are briefly described.

---

## Keywords

Early warning · Time prediction · Areal prediction · Computer simulation · Ring shear test

---

## 2.1 Introduction

The International Consortium on Landslides (ICL), the United Nations Educational, Scientific and Cultural Organization (UNESCO), the World Meteorological Organization (WMO), the Food and Agriculture Organization of the United Nations (FAO), the United Nations International Strategy for Disaster Risk Re-

duction (UNISDR), the United Nations University (UNU), the International Council for Science (ICSU), the World Federation of Engineering Organizations (WFEO) and others organized a Round Table Discussion to strengthen research and learning on landslides and related earth-system disasters for global risk preparedness and to create a new globally international programme on landslides. At this meeting at the United Nations University, Tokyo, from 18th to 20th January, 2006, the 2006 Tokyo Action Plan was adopted. Accordingly, a new IPL (International Programme on Landslides), jointly managed by ICL and

---

Kyoji Sassa  
Kyoto University Uje-Campus, UNITWIN Headquarters,  
e-mail: sassa@iclhq.org

seven other global stakeholders, was initiated. During this meeting after or between official sessions, many participants discussed possible collaborations. Participants from Korea, China, and Japan also discussed possible collaborative research. “Early Warning of Landslides” was agreed on as a joint research topic among the three countries. The International Consortium on Landslides then submitted a budget to the Ministry of Education, Sports, Culture, Science and Technology (MEXT), Japan, within an Asian Joint Research framework titled “Asian Joint Project: Early Warning of Landslides”, together with Korea, China, Indonesia, Thailand, Philippines and Japan. It was approved by MEXT in 2007 as a three-year project (April 2007–March 2010). It was also approved as IPL105 “Early Warning of Landslides” by the IPL Global Promotion Committee and it has had the status of an ongoing IPL project since 2007.

### 2.1.1 Concept of Early Warning (from Sassa & Picarelli, 2008)

Early warning is the whole of the actions to be taken before a catastrophic event, allowing individuals to act to avoid or reduce the impending risk. Lead time is the interval between the moment when the occurrence of the event becomes reasonably certain, and the moment of its actual occurrence. In recent years, early warning systems have been employed for protection against some natural risks. In some cases, such as severe meteorological events, volcanic eruptions and tsunamis, the warnings have proven to be very efficient, because the lead time available has been long enough to take actions such as evacuation, or protection of key structures and infrastructure. In other cases (such as for earthquakes, flash floods, rapid landslides), the lead time is so short that radical solutions for risk mitigation cannot be undertaken. In these cases, early warning can be adopted only for very limited goals or the warning signals must be sent well before the expected event, i.e. when its probability is high enough but it is not really certain. This last approach implies subjective decisions and can lead to false or missed alarms. In the case of rapid landslides, since the time between the onset of slope failure and its impact on exposed people and their possessions is typically in the order of tens of seconds, the problem is similar to the one posed by earthquakes, for which advanced procedures are being

developed, but even more complicated because often landslides may occur anywhere within a wide area that lacks any type of instruments able to recognize the occurrence of the event. Research in this field is active, even though it is just beginning.

### 2.1.2 Publication of Research Results of IPL 105 Early Warning of Landslides

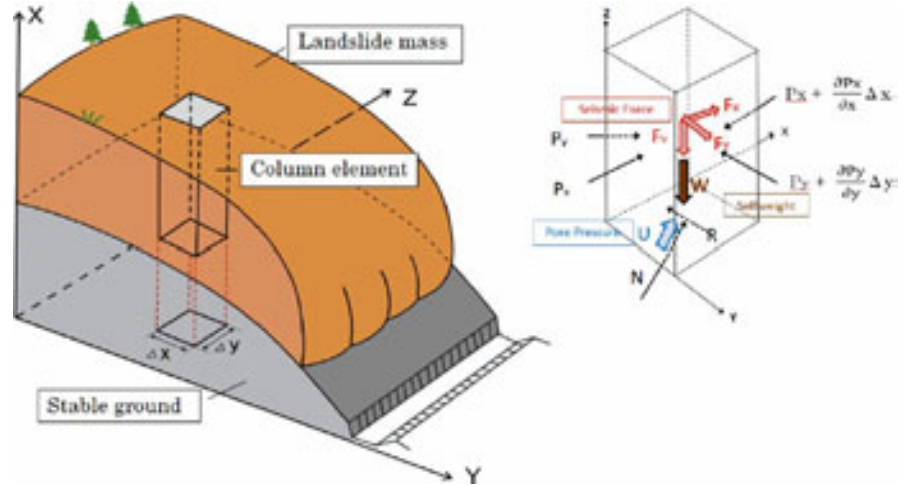
The activities of IPL105 include advanced research, social application of the scientific research, and capacity development. The advanced research from this project was presented to peer review for publication as original articles or technical notes in the journal *Landslides*. The accepted papers and other papers related to Early Warning were edited and published as a thematic issue on “Early Warning of Landslides” in *Landslides*, Vol. 7, No. 3. Some papers related to the social application of scientific research that were presented to the International Workshop on Early Warning of Landslide Disaster Risk Reduction in the Eastern Asian Region, from 30 November to 5 December 2009 in Kunming, China, were edited and published as a book: *Early Warning of Landslides* (Editors: Kyoji Sassa and Yin Yueping 2010) from Geological Publishing House in China. This chapter reports on the scientific part of this project in the following section.

## 2.2 Site and Areal Prediction

This research result was published in: “An Integrated Model Simulating the Initiation and Motion of Earthquake & Rain Induced Rapid Landslides and its Application to the 2006 Leyte Landslide” (Sassa et al., 2010).

The principal effective early warning for large landslides, especially those triggered by earthquakes, is site and areal prediction of landslide susceptibility. Large landslides seldom occur suddenly – they have commonly moved somewhat during previous rainfalls and earthquakes, and often they have precursor phenomena: namely sign of creeping, steps in the head, or shear zones in the side borders. Similarities in geology and geomorphology to nearby previously occurring landslides are also an indicator of a potential for large landsliding in the future. Identification of precursor phenomena is one target of research. Other targets are determining what conditions of rainfall and/or earth-

**Fig. 2.1** Basic principles of *LS-RAPID*. *Left*: A column element within a moving landslide mass. *Right*: Balance of forces acting on a column



quakes trigger landslides and what is the likely hazard area (landslide moving area). If these can be assessed, risk-preparedness action can be taken to reduce the effects of the disaster. This research presented a new computer simulation integrating the initiation process triggered by rainfalls and/or earthquakes and the progression to rapid motion due to strength reduction and the entrainment of deposits in the course of travel. This simulation model (*LS-RAPID*) was developed from the geotechnical model for the motion of landslides (Sassa, 1988).

### 2.2.1 Basic Principle of Simulation

The basic concept of this simulation is explained in Fig. 2.1. A vertical imaginary column within a moving landslide mass is considered. The forces acting on the column are 1) the weight of the column ( $W$ ), 2) seismic forces (vertical seismic force  $F_v$ , horizontal X-Y direction seismic forces  $F_x$  and  $F_y$ ), 3) lateral pressure acting on the side walls ( $P$ ), 4) shear resistance acting on the bottom ( $R$ ), 5) the normal stress ( $N$ ) acting on the stable basal substrate as a reaction of the normal component of the column weight, and 6) pore pressure acting on the bottom ( $U$ ).

The landslide mass ( $m$ ) will accelerate at ( $a$ ) given by the sum of these forces: driving force (column weight + seismic forces) + lateral pressure + shear resistance

$$am = (W + F_v + F_x + F_y) + \left( \frac{\partial P_x}{\partial x} \Delta x + \frac{\partial P_y}{\partial y} \Delta y \right) + R \quad (2.1)$$

Here, the resistance  $R$  includes the effects of forces of  $N$  and  $U$  in Fig. 2.1 and works in the upward direction of the maximum slope line before motion, and in the opposite direction to landslide movement during motion.

The slope angle varies with the position of the column within landslide mass. All stresses and displacements are projected to the horizontal plane and calculated on the plane (Sassa 1988).

### Effect of Shear Strength Reduction from the Pre-Failure State to Steady State Motion

The initiation process of this model consists of the following four sub-processes:

1. An initial state in which the soil layer is in a stable condition under the friction coefficient at peak strength ( $\tan \phi_p$ )
2. Failure (the instant of peak shear resistance) will occur due to a rise of ground water level during rain, seismic loading during an earthquake, or a combination of ground-water rise and seismic loading.
3. Transient state from peak to steady state in which pore-pressure generation and resulting shear strength reduction proceeds in tandem with shear displacement.
4. Steady state, in which the landslide mass moves with no further strength reduction.

Figure 2.2a,b presents examples of test results of silica sands in an undrained ring shear apparatus. Shear resistance reaches its peak value within 1–2 mm shear displacement, and both cases reach a steady state between 10–5,000 mm of shear displacement. Strength reduc-

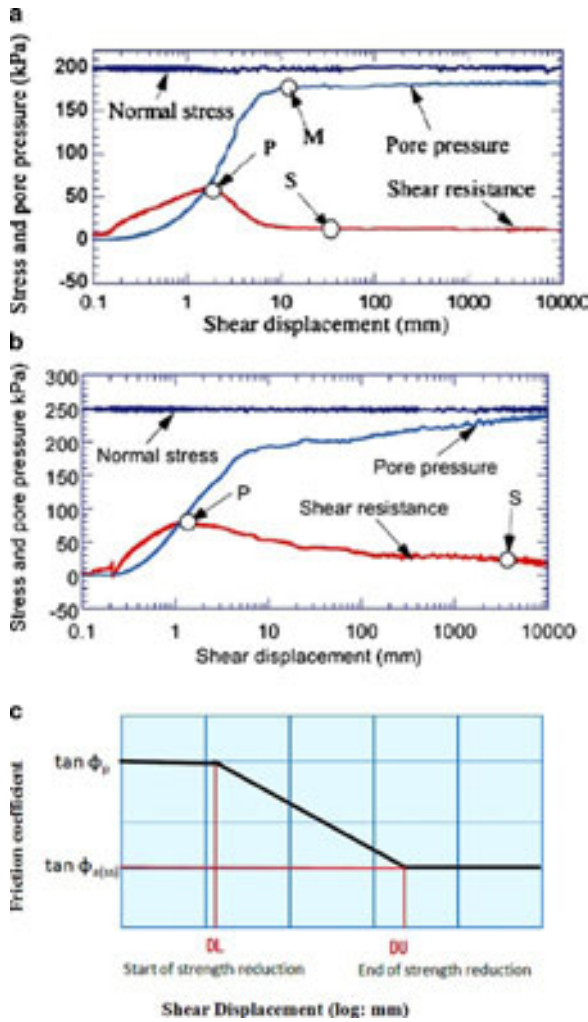


**Fig. 2.2** Model of shear strength reduction in the progress of shear displacement. **a, b** Test examples, **c** modeling based on testing

tion after 1,000 mm is very small, so it is regarded as reaching a steady state between 10–1,000 mm.

In reference to these experimental results, the shear behavior from the pre-failure state to a steady state of motion through the transient state can be approximated as shown in Fig. 2.2c. Namely the friction angle at peak ( $\phi_p$ ) is kept in the pre-failure state until the shear displacement DL (Point of failure, Start of strength reduction). In real slopes, shear stress does not start from zero. It is relatively close to the peak, although the level is unknown. Shear strength reduces from DL to DU (end of strength reduction) in the shear displacement along a line in the logarithmic axis. A steady-

state landslide motion will start under the apparent friction coefficient ( $\tan \phi_{a(ss)}$ ) after DU in the shear displacement. Expressing the shear displacement as D, the friction coefficient has the following three stages:

1. Initial deformation stage before failure ( $D < DL$ ):  $\tan \phi_a = \tan \phi_p$
2. Stage of steady-state motion ( $D > DU$ ):  $\tan \phi_a = \tan \phi_{a(ss)}$
3. Stage of transient state ( $DL < D < DU$ ):  $\tan \phi_a = \tan \phi_p - \frac{\log D - \log DL}{\log DU - \log DL} (\tan \phi_p - \tan \phi_{a(ss)})$ .

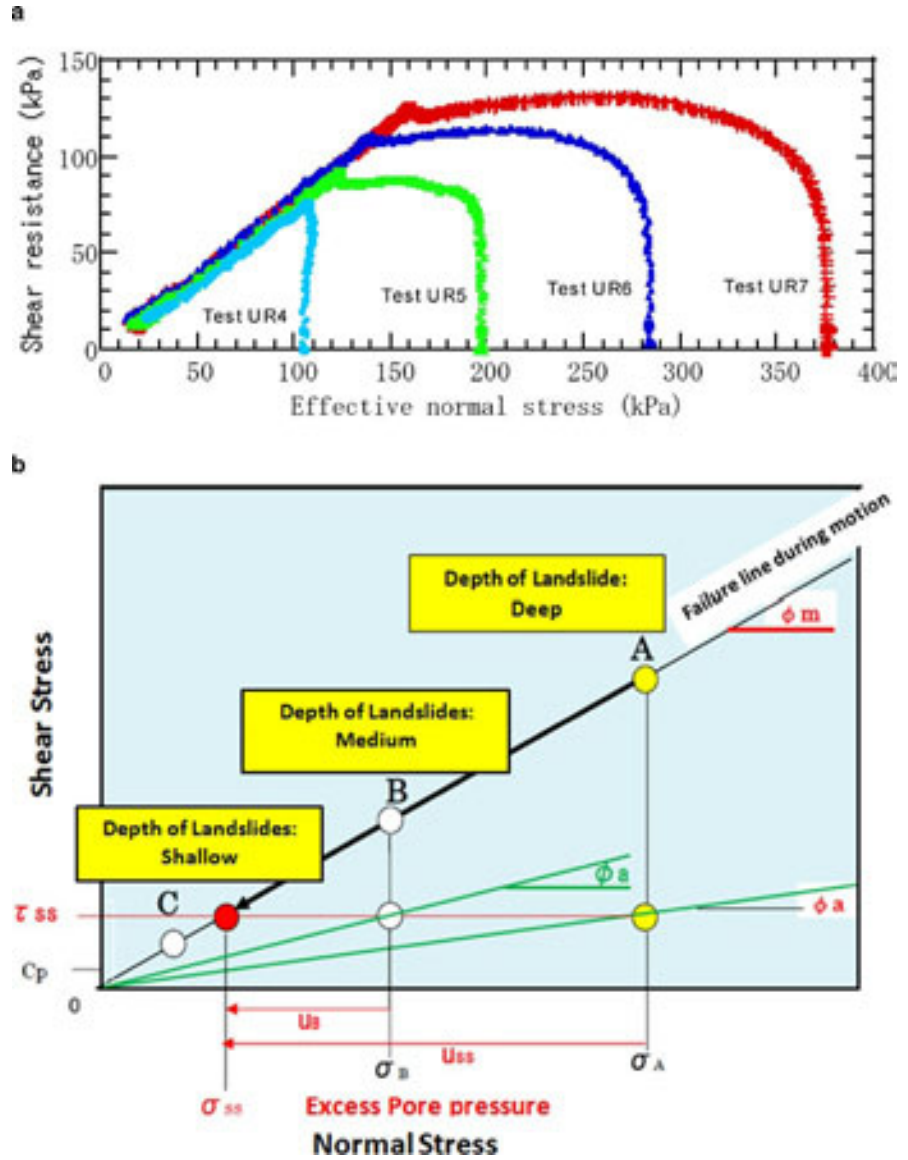
### Effect of Soil Depth on the Apparent Friction Coefficient

The normal stress at steady state ( $\sigma_{ss}$ ) is independent of the level of loaded normal stress. Figure 2.3a shows an example of weathered granitic soils taken from the Osaka formation in which the Nikawa landslide occurred, killing 34 persons in Nishinomiya city, Hyogo Prefecture, Japan. All soils with different normal stress reached the same steady-state shear resistance in the undrained ring shear test. No further grain crushing and volume reduction will occur under this critical normal stress. Using this relation, the apparent friction coefficient can be determined as a function of soil depth as illustrated in Fig. 2.3b. Where the landslide mass has a greater depth, the mobilized apparent friction coefficient ( $\tau_{ss}/\sigma_A$ ) is smaller, as shown by point A. However, as the depth of landslide mass becomes smaller, the mobilized friction coefficient becomes greater, as shown by point B. At a lower normal stress than the normal stress at steady state ( $\sigma_{ss}$ ), the apparent friction coefficient is the same as the friction coefficient during motion ( $\tan \phi_m$ ) as shown by point C. When the motion of the landslide mass accelerates and becomes fast, the landslide depth will decrease; in this case the apparent friction coefficient will increase.

### Examination of the Performance of Initiation Process Comparing to the Slope Stability Analysis

The performance of the initiation process of *LS-RAPID* is examined by applying it to a simple imaginary slope. The imaginary slope is composed of three parts – flat ground at the top, a steep slope in the middle and a gentle slope at the bottom. The area of simulation is 350 m wide and 440 m long, the size of mesh is 10 m, the maximum vertical depth of landslide

**Fig. 2.3** A constant steady-state shear strength in different normal stress and its effect on mobilized friction angle. **a** Test results, **b** the effect on landslide motion of different depths of landslide mass during motion



is 40.53 m, the total landslide volume is 231,300 m<sup>3</sup>. The landslide body shape is modeled as an ellipsoid.

The characteristic of *LS-RAPID* is the expression of strength reduction during deformation and the progressive failure. A relatively strong slope was considered which may fail due to a high pore pressure ratio within the bedrock or the combined effects of seismic loading in addition to a moderate pore pressure ratio.

The values of  $\tan \phi_p = 0.8$ ,  $C_p = 50$  kPa,  $\tau_{ss} = 50$  kPa,  $k = 0.5$ ,  $B_{ss} = 0.99$ ,  $\tan \phi_m = 0.60$  were assigned the entire simulation area. As the parameters of the shear-resistance reduction model, the shear

displacement at the start of reduction  $DL = 10$  mm, and the shear displacement reaches steady-state shear resistance  $DU = 1,000$  mm were assumed for the result of undrained ring shear testing (Fig. 2.2) for a hypothetical case. A local failure and shear strength reduction may start at a mesh (site) in which the shear displacement firstly reaches  $DL = 10$  mm, then it may develop to a progressive failure.

In order to compare this simulation result to the standard limit equilibrium slope stability analyses (such as the Fellenius, Bishop, Janbu, Spenser, Morgenstern–Price methods) a large enough shear dis-



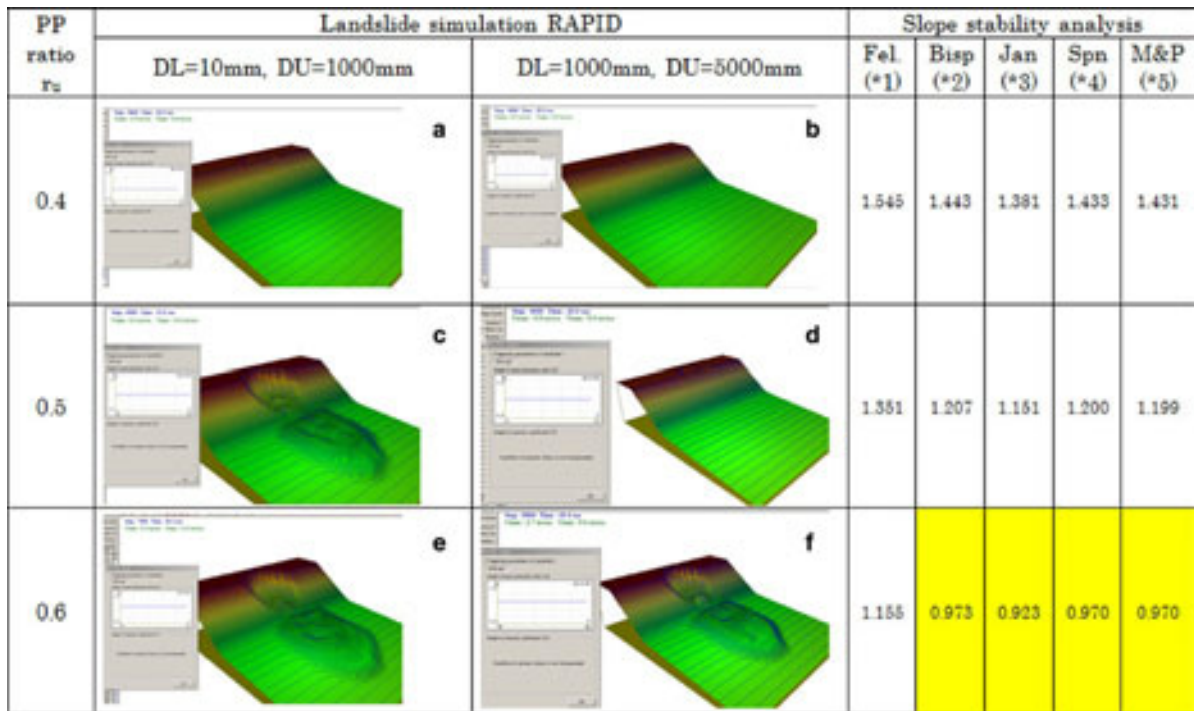


**Fig. 2.4** Landslide initiation in RAPID and Slope Stability Analysis  $\tan \phi_p = 0.8$ ,  $C_p = 50$  kPa,  $\tau_{ss} = 50$  kPa,  $k = 0.5$ ,  $Bss = 0.99$ ,  $\tan \phi_m = 0.60$ , mesh: 10 m, area:  $350 \times 440$  m,

$\alpha = 0$ , min. cal. time = 10 s. Blue color line is the border of moving mass \*1: Fellenius, \*2: Bishop simplified, \*3: Janbu simplified, \*4: Spenser, \*5: Morgenstern–Price

placement for DL and DU was assumed to be 2 m and 5 m respectively. The limit equilibrium slope stability analysis does not consider progressive failure, but fails at once. The large shear displacement DL is effectively to restrain the effect of shear-resistance reduction and progressive failure in the initiation process. The simulation results are shown in the form of a 3D view in Fig. 2.4. The contour interval is 2.0 m. The red line shows the area of moving landslide mass. The red color will appear when/where the velocity at a mesh exceeds 0.5 m/s.

#### DL = 10 mm, DL = 1,000 mm

In the case of  $r_u = 0.4$  (Fig. 2.4a), only two small areas at the top of the slope showed a slight movement and two red colored circles were observed, but no further progressive failure appeared. For  $r_u = 0.5$  and 0.6, rapid landslide motion appeared as shown in Fig. 2.4c,e.

#### DL = 2,000 mm, DU = 5,000 mm

No motion appeared for  $r_u = 0.4$ , a limited deformation appeared for an instant in the case of  $r_u = 0.5$

as shown Fig. 2.4b,d. A rapid landslide occurred for  $r_u = 0.6$  (Fig. 2.4f). The threshold of landslide initiation is between  $r_u = 0.4$  and 0.5 for smaller DL-DU, and it is between 0.5 and 0.6 for greater DL-DU.

#### Time

Simulation is stopped when zero velocity appears for all meshes. Time in the figure shows the time from the start to the end of motion. 10 s for a, b, d was the pre-determined minimum calculation time, because the initial velocity is zero, and a certain time duration is necessary to determine whether movement will start or not.

For the central section of this landslide mass, two-dimensional slope stability analyses were implemented using the stability analysis software “Slide, version 5” by Rocscience. The same shear strength parameters at the peak and also the same pore pressure ratio ( $\tan \phi_p = 0.8$ ,  $C_p = 50$  kPa,  $r_u = 0.4, 0.5, 0.6$ ) were given for all stability analysis methods. The calculated safety factors for 1: Fellenius, 2: Bishop simplified, 3: Janbu simplified, 4: Spenser, 5: Morgenstern–Price methods are shown in the right

column of Fig. 2.4. The onset of landslide motion, namely the unit safety factor ( $FS = 1.0$ ) appears when the value of  $r_u$  is between 0.5 and 0.6 for four models. For the Fellenius method, the factor of safety becomes unity when the value of  $r_u$  is between 0.6 and 0.7. Therefore, except for the Fellenius method, the threshold of stability ( $FS = 1.0$ ) is similar to the threshold indicated by *LS-RAPID* in the case of long shear displacement (2 m) until the start of shear strength reduction. The difference between *LS-RAPID* and the Limit Equilibrium Slope stability analysis comes mainly from the consideration of local shear and progressive failure or the overall shear for the whole landslide body at once. The difference between three-dimensional analysis and two-dimensional analysis cannot be discussed in this examination.

### Simulation of the 2006 Leyte Landslide

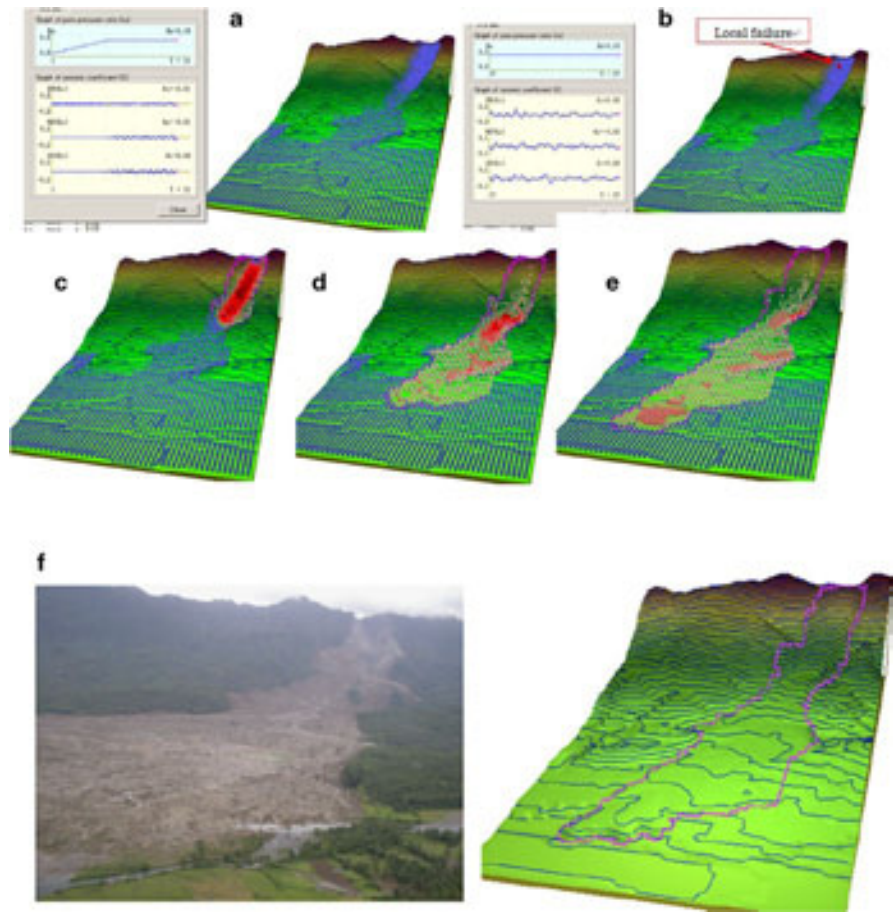
An important parameter in the 2006 Leyte landslide is the steady-state shear resistance ( $\tau_{ss}$ ). The steady-state shear strength is very low, less than 10 kPa, as measured by the undrained ring shear apparatus on a volcanoclastic debris sample taken from the base of the Leyte flow mound. The testing condition is 100 % saturation and the loading stress corresponds to 35 m depth (much shallower than reality). The sample used may be more weathered than that in this deep landslide body. We selected  $\tau_{ss} = 40$  kPa as a practical value for this landslide. Various combinations of values of factors can be considered. We estimated that the peak friction and peak cohesion before motion in the source area should be high ( $\tan \phi_p = 0.9$ ,  $C_p = 100\text{--}300$  kPa). The shear displacement for shear-strength reduction was estimated as  $DL = 100$  mm,  $DU = 1,000$  mm based on the test result of the sample. In the trial simulation, no landsliding occurred for a pore pressure ratio  $r_u = 0.10, 0.15$ . However, a value of  $r_u = 0.16$  caused a rapid landslide. Around 30 % saturation in this source area is the critical value to trigger a landslide without an earthquake. Then, various magnitudes of seismic shaking, using the wave forms of EW, NS and UD recorded at Maasin, Leyte were assigned, in addition to a pore-pressure ratio of 0.15. The threshold value to initiate a rapid landslide was between  $K_{EW} = 0.11$  and 0.12; we therefore used  $K_{EW} = 0.12$ . Using the ratio of magnitudes of seismic records of EW, NS and UD,  $K_{NS} = K_{UD} = 0.061$ . The seismic shaking of three directions of EW, NS and UD were given in this sim-

ulation. Unstable deposits 3 m thick are assumed in the alluvial deposit area. Figure 2.5a shows the unstable soil deposits (initial landslide body) in the source area and also unstable deposits in the alluvial flat area (shown in blue). The critical height ( $\Delta h_{cr} = 0.5$  m) to reduce shear strength from peak to the steady state was given. A series of motions was presented for the case of  $K_{EW} = 0.12$ ,  $K_{NS} = K_{UD} = 0.061$ ,  $r_u = 0.15$  in Fig. 2.5a–e. Figure 2.5a:  $r_u$  rises to 0.15 and an earthquake will start but cause no motion. Figure 2.5b: Continued earthquake loading (Max  $K_{(EW)} = 0.12$ ,  $K_{NS} = K_{UD} = 0.061$ ) triggers a local failure (red color mesh), Fig. 2.5c: An entire landslide block is formed and moving, Fig. 2.5d: The top of the landslide mass moves on to the alluvial deposits, Fig. 2.5e: Deposition. The air photo taken from a helicopter (left) and the simulation results presented in 3D view from a similar angle (right) are presented in Fig. 2.5f. The travel distance and the major part of landslide distribution were well reproduced. The secondary debris flow and muddy water spread to the left in the photo and field observation. These were not present in the computer simulation.

The research results are summarized in the followings.

1. A new computer simulation model (*LS-RAPID*) was developed. It integrated the *stability analysis* from a stable state to the failure (initiation of landslide) triggered by pore pressure increase and/or seismic loading, and a *dynamic analysis* for the post-failure motion. The reduction of shear resistance from the peak to the steady-state was modeled and incorporated in this programme.
2. The computer programme could reproduce the progressive failure of the slope because shear resistance starts to decrease where or when the shear displacement reaches the threshold value of shear displacement.
3. Comparison of *LS-RAPID* with conventional limit equilibrium stability analyses of Bishop, Janbu, Spensor, Morgenstern and Price showed that landslides can be initiated at a lower pore-water pressure ratio in *LS-RAPID* because of progressive failure. The threshold value of the start of shear strength reduction was changed from 10 mm (estimated from experiments) to 2,000 mm (a large value) to restrain the initiation of progressive failure. In this case, the border between motion and no motion in *LS-RAPID* was the same as the threshold

**Fig. 2.5** Simulation of the Leyte landslide Mesh: 40 m, Area:  $1,960 \times 3,760$  m, contour line: 20 m. 3 m unstable deposits in the alluvial deposit area (blue)



indicated by conventional limit equilibrium stability analyses.

4. The new computer simulation was applied to the 2006 Leyte landslide based on the values measured in laboratory and monitored seismic records. Key parameters of the steady state shear resistance was decided, based on the result of laboratory tests, though it was not complete because the loaded normal stress is different due to the limited capability of the apparatus. The computer simulation reproduced a rapid landslide with a similar travel distance and distribution area, which was triggered by a pore water pressure ratio of 0.15 and a small seismic shaking of  $K_{EW} = 0.12$ , and  $K_{NS}$  and  $K_{UD} = 0.061$ , using the seismic wave forms recorded at the Maasin observatory. The simulation result almost corresponded that the rapid landslide triggered by a small nearby earthquake of  $M_s = 2.6$  in 5 days after the consecutive heavy rains over 3 days with an intensity of over 100 mm/d.

### 2.3 Time Prediction from Satellite Monitoring

This research result was published in: “A distributed hydrological-geotechnical model using satellite-derived rainfall for shallow landslide warning in a large catchment” (Apip et al., 2010).

This paper described the application of a hydrological-geotechnical modeling system using satellite-based rainfall estimates for a shallow landslide prediction system. The physically based distributed model has been developed by integrating a grid-based distributed kinematic wave rainfall-runoff model with an infinite slope stability approach. The model incorporated satellite-based, near real-time, *half-hourly* CMORPH global rainfall data prepared by NOAA-CPC.

The study was primarily concerned with shallow landslides referred to as debris flows, which are rapidly moving flows of mixed water, soil and rock. Because



these landslides are caused primarily by heavy rainfall on saturated hillslopes, this study examined them by mapping areas of potential slope instability over the river catchment. The modeling system was designed for analyzing the hydrological responses that induce slope instability and characterizing the susceptibility of a slope to shallow-landslide generation. A near real-time satellite-derived rainfall product (CMORPH global rainfall data) was used in the system to evaluate the application of the system for real-time prediction and warning of flood-associated shallow landslides based on varying slope instability.

The method combined two types of information to identify “where” and “when” shallow landslides may occur in a catchment: First, a slope stability model was used to derive a time-invariant spatial distribution map of the areas susceptible to slope instability, in which the catchment area was divided into stability classes according to critical relative soil saturation. It was designed to portray the effect of quasi-static land surface variables (geometric characteristics of the slope, geotechnical properties, and strength parameters of the soil) on slope instability without considering the dynamic factors triggering it. The areas defined as potentially stable/unstable were targeted as the areas for slope instability analysis. The long-term spatial pattern of recorded landslide locations (1985–2008) was overlaid to calibrate the model output. Second, the produced map was linked to varying hydrologic responses to provide a time-varying estimate of slope movement susceptibility in response to real-time rainfall intensities. The hydrological model estimated the dynamics of soil saturation in each grid element, which was then used to update the state of relative soil saturation and to assess local slope instability for those areas classified as potentially stable/unstable. Potential instability was regarded as increasing when the soil saturation became higher than a critical level. The slope instability information formed the basis for issuing a shallow-landslide warning according to the risk level, which depended on the period of soil saturation above the critical level. Figure 2.6 shows the framework of model development for the shallow-landslide prediction system.

A one-dimensional physically-based distributed hydrological model based on a grid-cell kinematic wave rainfall-runoff model was developed for simulating hydrological responses and soil saturation. In this modeling framework, catchment topography was

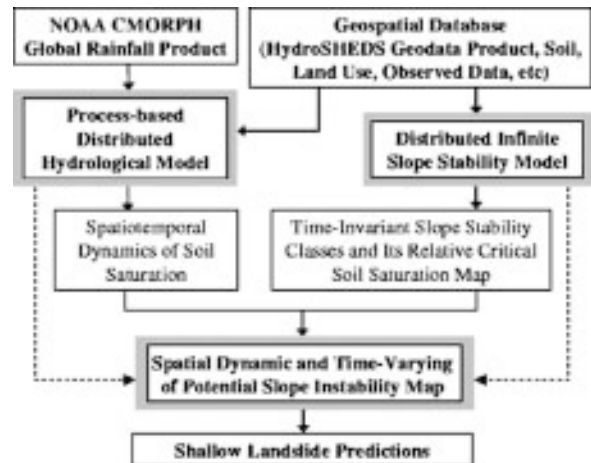


**Fig. 2.6** Modeling framework for the shallow-landslide prediction system

based on a digital elevation model (DEM) that was divided into an orthogonal matrix of square grid cells. A square area on a node point of a DEM was considered as a subcatchment, which was called a grid cell. The river catchment was modeled as a network of grid cells. Each grid cell received flows from up-slope grid cells and rainfall on it. These grid cells were connected to each other with a drainage path defined by the steepest of eight directions. Discharge and water depth diffuse to the next grid cell according to a predefined eight-direction flow map and a routine order determined in accordance with the DEM and river-channel network data. The hillslope flow was routed and passed to the river flow routing model; then the river flow was routed to the outlet (Fig. 2.7). The slope stability model was developed, based on the concept of an infinite slope model, using the factor of safety (FS) that incorporated a failure surface. The following were assumed: (a) failure was the result of translational sliding, (b) the failure plane and water table were parallel to the ground surface, (c) failure occurred as a single layer, (d) the failure plane was of infinite length, and (e) the impacts of adjacent factors were not taken into account. For hillslopes, the safety factor generally was represented as the ratio of the available resisting force (shear strength) to the driving force (shear stress). Instability occurred when the shear strength of a soil layer became smaller than the shear stress acting on the soil. The governing equation of the safety factor used in this study was based on a Mohr–Coulomb failure law.

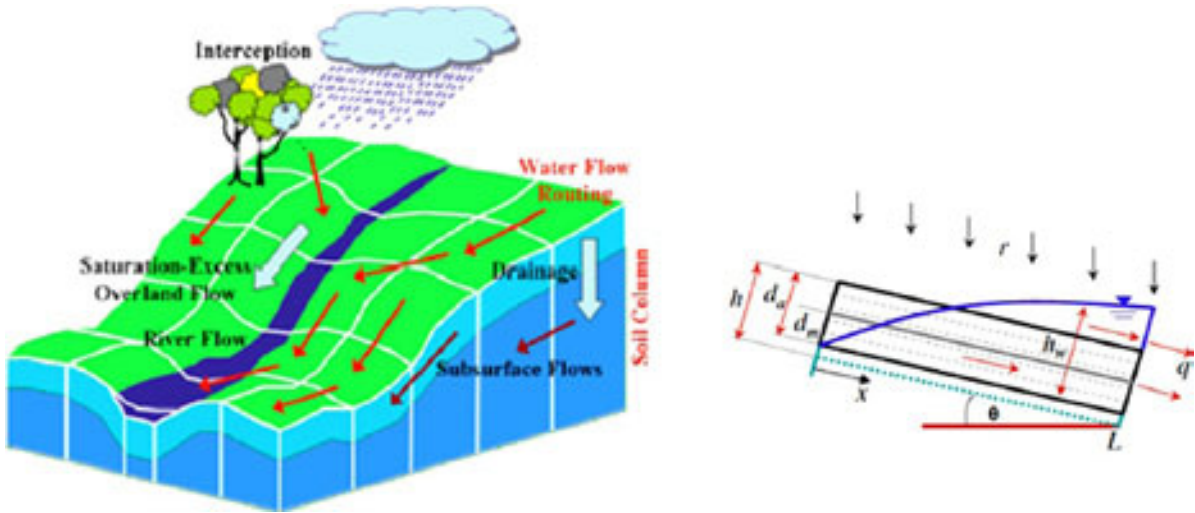
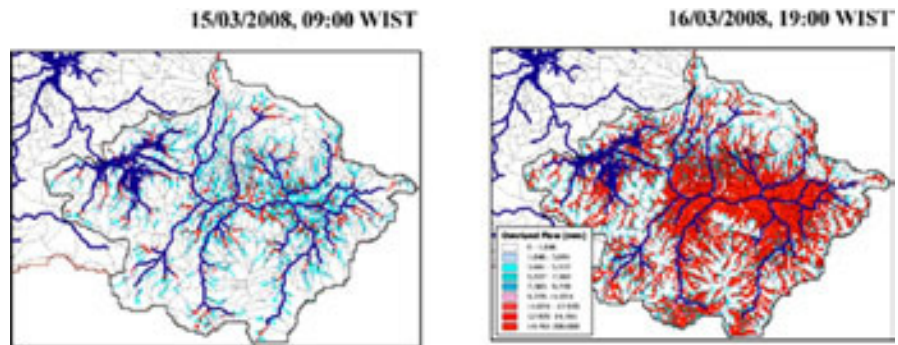


**Fig. 2.7** Illustrative grid-cell distributed hydrological model, with a thin soil mantle of constant hydraulic conductivity overlying impermeable bedrock of an infinite slope

**Fig. 2.8** Two maps of predicted saturated excess overland flow depth with respect to NOAA CMORPH rainfall input data on 15 and 16 March 2008 in the upper Citarum River catchment, Indonesia.



An understanding of how the distributed hydrological model worked in processes related to soil saturation for the 15–16 March 2008 rainfall events generated from CMORPH rainfall estimates is shown in Fig. 2.8. The figure shows two selected views of the 90-m grid squares predicted to have saturated excess overland flow over the study catchment. During a particular rainfall event, the saturated excess overland flow zones spread from flatter areas (middle part) to topographically convergent hillslopes where slope failure often occurs. Figure 2.8 shows clearly that the central part of the area was inundated.

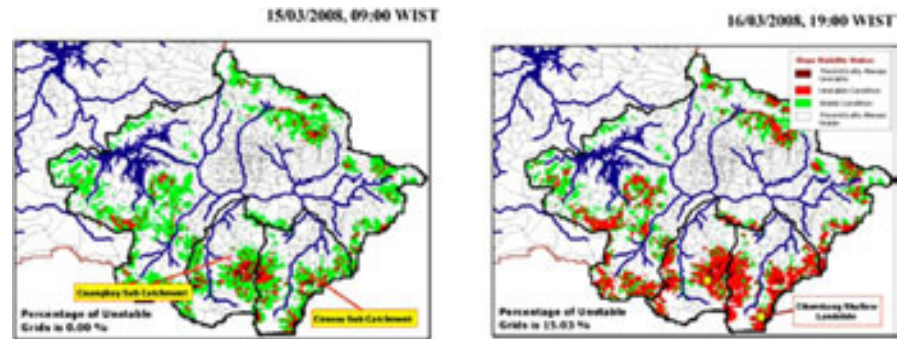
Figure 2.9 presents two examples of predicted time-varying slope stability over all areas characterized as potentially stable/unstable. The simulation period was from 0000 hours WIST on 15 March 2008 to 2300 hours WIST on 16 March 2008. Most of these potentially stable/unstable areas were predicted to be

unstable (red color) at some rainfall rate. The pattern of predicted instability, however, changed systematically with increasing rainfall. The rainfall rates increased the water storage depth to levels sufficiently higher than the threshold level to cause slope failure. Figure 2.9 shows that for the 15 March or 16 March events, several hours before the landslides the model predicted that some grids over and near to the two observed shallow landslides were in an unstable condition.

## 2.4 Safety Factor Change in Shallow Landslides from Satellite Monitoring

This research result was published in: “Prototyping an experimental early warning system for rainfall-induced landslide in Indonesia using satellite remote sensing and geospatial datasets” (Liao, et al. 2010).

**Fig. 2.9** Examples of the time-varying slope stability condition on 15–16 March 2008 in the upper Citarum River catchment, Indonesia. (green color areas are stable and red color areas are unstable). Landslides occurred in the two locations indicated by yellow squares.



An early warning system has been developed to predict rainfall-induced shallow landslides over Java Island, Indonesia. The prototype early warning system integrated three major components: (1) a susceptibility mapping and hotspot identification component based on a geospatial database (topographical information, maps of soil properties, and local landslide inventory, etc.); (2) a satellite-based precipitation monitoring system (<http://trmm.gsfc.nasa.gov>) and a precipitation forecasting model (i.e., Weather Research Forecast); and (3) a physically based, rainfall-induced landslide prediction model SLIDE. The system utilized the modified physical model to calculate a factor of safety that accounted for the contribution of rainfall infiltration and partial saturation to the shear strength of the soil in topographically complex terrains. In use, the land-surface “where” information is integrated with the “when” rainfall triggers by the landslide prediction model to predict potential slope failures as a function of time and location. In this system, geomorphologic data were based primarily on 30m Advanced Spaceborne Thermal Emission and Reflection Radiometer (ASTER) data, digital elevation model (DEM), and 1 km soil maps. Precipitation forcing came from both satellite-based, real-time National Aeronautics and Space Administration (NASA) Tropical Rainfall Measuring Mission (TRMM), and Weather Research Forecasting (WRF) model forecasts.

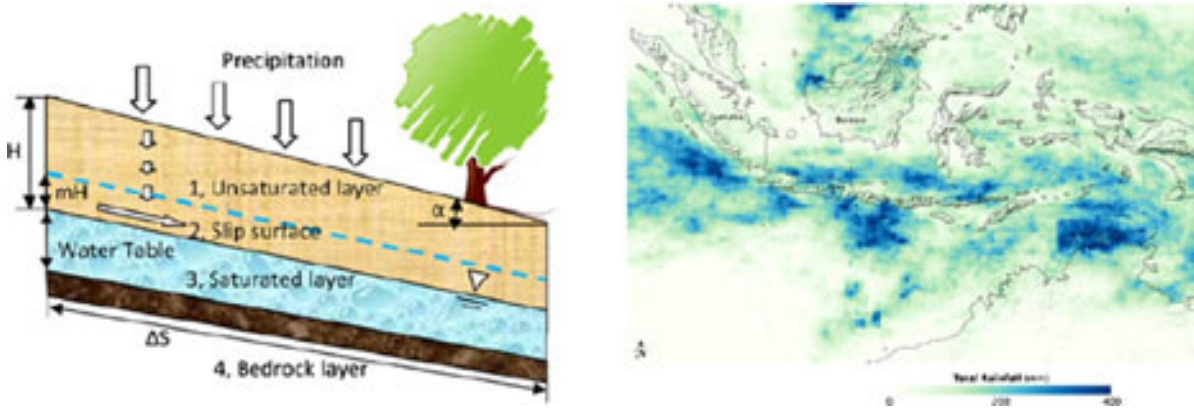
Figure 2.10 (left) shows the model used to calculate the factor of safety of slope; it highlights the destabilizing forces from the downward flow of water and the contribution of partial saturation to the shear strength of the soil. Figure 2.10 (right) is an image of rainfall accumulation by NASA TRMM-based Multi-satellite Precipitation Analysis over Java Island in late December, 2007,

posted by Earth Observatory, NASA on January 8, 2008.

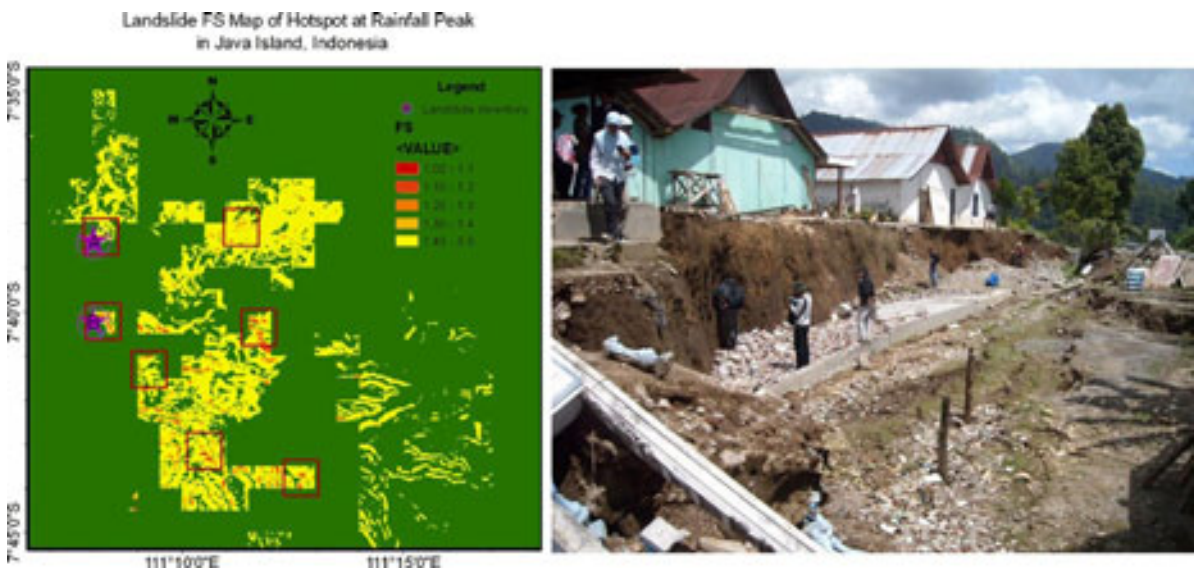
Factor of safety (FS) values were calculated over the area in the hotspot susceptibility map. A factor-of-safety map at the peak of the rainfall event is shown in Fig. 2.11 (left). Results shows that during the peak of the typhoon rainfall, FS values below 1.2 account for 25.06 % of the land areas that rank in susceptibility categories of high and very high. For FS values below 1, seven areas shown as red squares in Fig. 2.11 (left) were predicted to have landslides. According to reports of local news, two out of the seven square areas had large landslides that killed more than 65 people. The other five predictions were not validated due to lack of landslide information in the remote areas with no residences. The photo of the landslide that occurred at B is shown in Fig. 2.11 (right).

Figure 2.12a denotes a predicted slope failure at the 23rd time-step (shown by the yellow arrow) in the TRMM rainfall series, where the Factor of safety is below the critical value indicated by the dash line. FS values decrease after rainfall reaches its peak value of approximately 50 mm/3 h. The total rainfall keeps accumulating until it reaches above 150 mm. Although the prediction time shows a 3-hour delay, it is still in agreement with the date of the event occurrence reported in local news on December 26, 2007. In addition to the TRMM rainfall, the model has been run using WRF precipitation to investigate how well the model would perform in the Early Warning System. Figure 2.12b shows that the WRF rainfall series indicated a much lower intensity compared with TRMM for the same event over the landslide site B shown in Fig. 2.11 (right). The WRF rainfall gives a storm event accumulation of rainfall of 150 mm, however, which agrees with the TRMM values. In the WRF-driven simulation, FS values show the same trend in





**Fig. 2.10** Left: A slope model for calculation of the factor of safety and right: an image of rainfall accumulation by NASA TRMM-based Multi-satellite Precipitation Analysis



**Fig. 2.11** Left: Factor of safety (FS) map by a 30-meter ASTER DEM showing the locations of two observed landslides and seven predictions at the peak time of the rainfall series and Right:

the photo of the headscarp of landslide (B) which occurred at Tengklik Sub-Village, Tawangmangu, Karanganyar Regency, Java, Indonesia.

time, with the lowest value of 0.99 indicating a landslide.

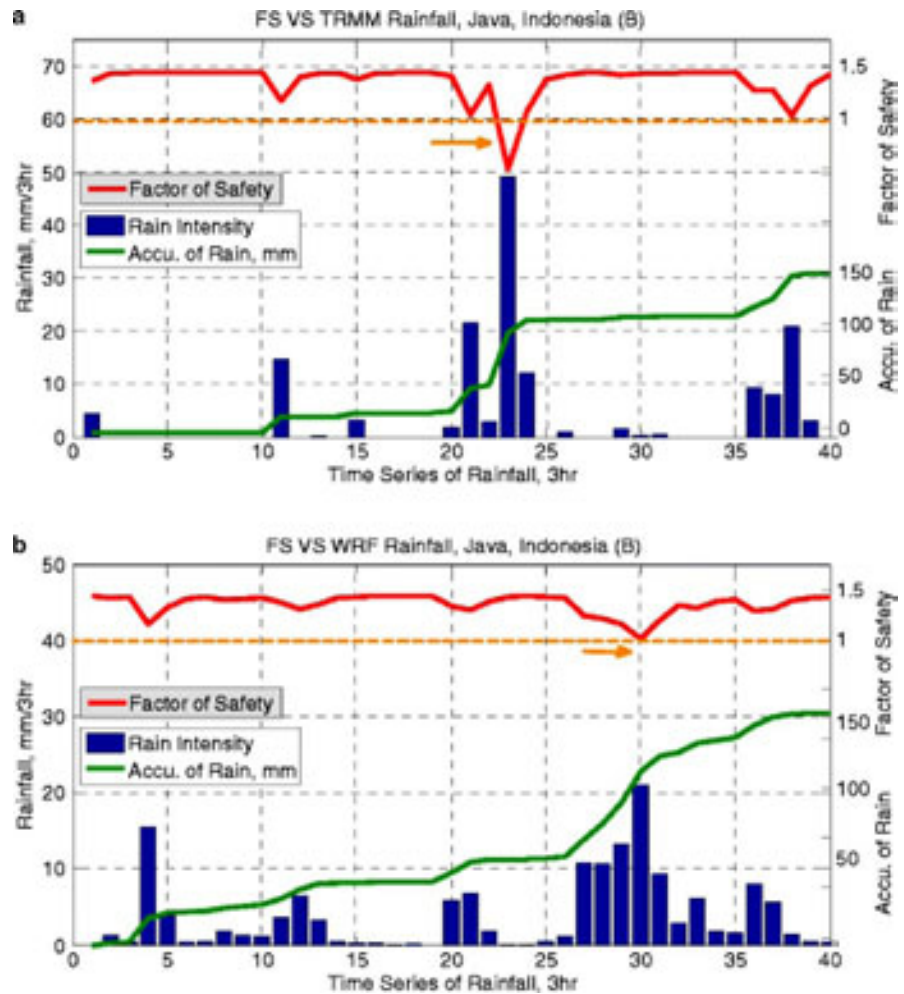
This paper used the rainfall monitoring from satellite each 3 hours, which is longer than the half-hourly CMORPH global rainfall product used in the paper by Apip et al. (2010). In Indonesia and many other developing countries, radar rainfall monitoring systems do not cover the whole area of the country. The use of satellite data will be important to provide rainfall information for early warning of rain-induced landslides.

## 2.5 Others

One of the targets of the Asian Joint Project was technological transfer and capacity development. But this project was a programme for Asian Network by the Ministry of Education, Culture, Sports, Science and Technology (MEXT) of Japan and budgets did not include donation of equipment. However, long-span extensometers which have around 40–80 m span



**Fig. 2.12** **a** FS VS TRMM rainfall in the landslide B;  
**b** FS VS WRF rainfall in the landslide B



over roads, small trees and houses, rain gauges, pore-pressure monitoring, cameras, and early warning and data-transfer systems were donated as consumables which may be damaged by landslide movements. The systems were set in two sites shown in Fig. 2.11 (left). Figure 2.13 shows one of the sites – the left-top presents an air photo taken from a balloon by Gadjah Mada University staff, and the map was made from these photos. The red and blue lines show two of the installation lines. The right photos of Fig. 2.13 show installation work on the extensometers; the left-bottom is the monitoring data. In the kick-off meeting and joint field investigation in 2007, we estimated that this slope might fail in the near future; we then agreed to install extensometers at this site. We purchased and installed them. However, our prediction was too precise – the site moved immediately after (and even

during) installation. The movement data was saturated, and one of the extensometer poles was buried, one pole was inclined and one pole remained. Three weeks after this landslide event, the system was moved to P4-P5-P6 points nearby.

The Gadjah Mada University (ICL member), together with an ICL group, organized an evacuation drill based on early warning from the extensometers with the participation of the project group from Japan, China, Korea, Philippines and Thailand. Figure 2.14 (left) is the photo showing an explanation to residents, including children, in the villages. The Gadjah Mada university group developed extensometers with a simple early warning system. Japanese early warnings are issued based on either displacement speed or displacement/hour or accumulated displacement. However, the system developed by the Gadjah Mada University was

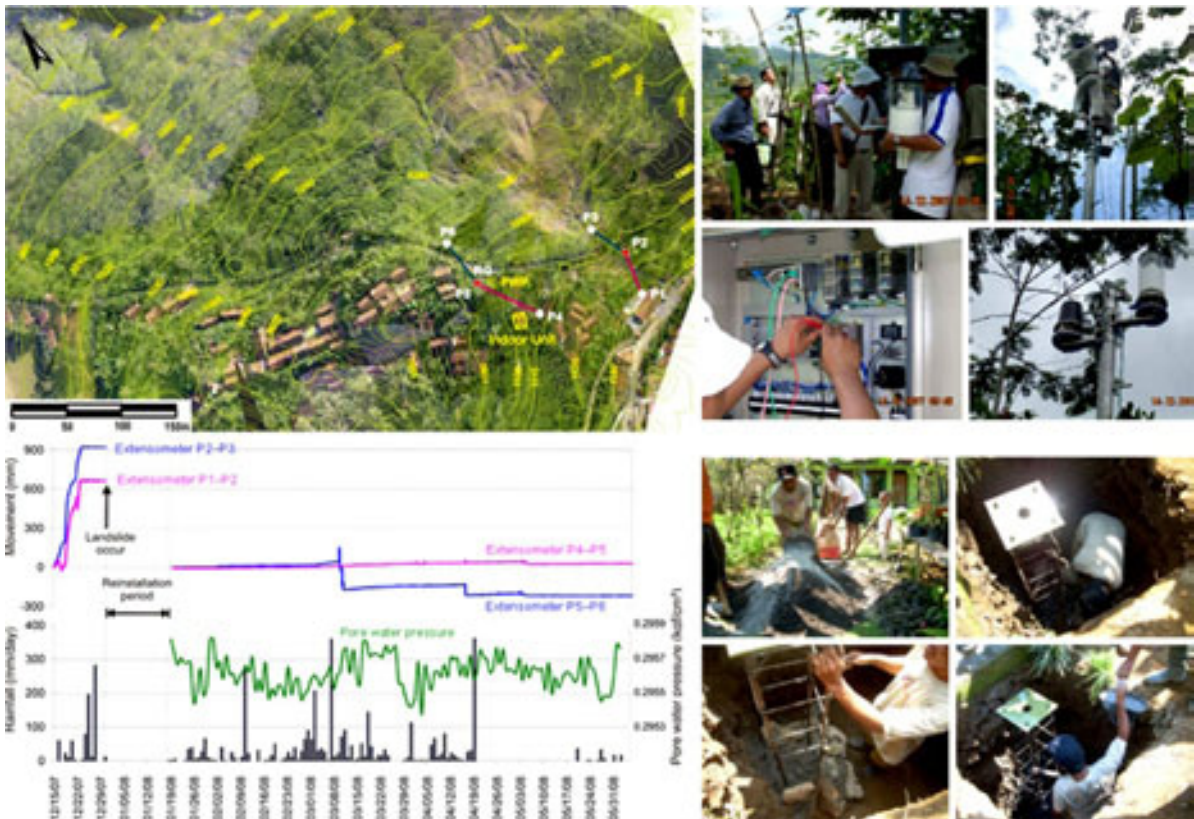


**Fig. 2.13** Long-span extensometers during installation and the initial monitoring data in Karanganyar Regency in the central Java, Indonesia.

even simpler – the alarm is issued when a wire moves to a certain limit. The China Geological Survey developed further simple early warning systems without monitoring at all (top-right), and also a crack gauge without a recording system installed crossing a crack which issues sound when triggered by both a certain parallel or normal displacement. Various systems were developed and around 100,000 sets were installed over China because of the simplicity and inexpensive price.

## 2.6 Conclusion and Social Impact

This Asian joint project was conducted by Indonesia, China, Japan, Korea, Philippines and Thailand. The scientific research has been published in the thematic issue of *Early Warning of Landslides*, *Landslides*, Vol. 7, No. 3. Thirteen papers presented in the joint workshop held in Kunming were published as a book

of *Early Warning of Landslides* from China Geological Publishing House. Session 13 of the First World Landslide Forum was “Monitoring, prediction and early warning” which was published in *Landslides-Disaster risk reduction* (Sassa et al., 2008).

The MEXT programme was reviewed in 2010 at the completion of the project. The evaluation was A in all aspects – Integrated evaluation: A, Rate of achievement of objectives: A, Results of project: A, Planning and implementation method: A, Sustainability and further development possibility after the project: A. This project got the highest evaluation. The members of this project are ICL members in Japan (ICL Headquarters and Kyoto University-Disaster Prevention Research Institute), China (China Geological Survey), Indonesia (Gadajah Mada University) and Korea (Korean Institute of Geoscience and Mineral Resources).

This project evaluation result was released at the evaluation period of the application from ICL headquarters, together with three ICL member organiza-

**Fig. 2.14** Japan-Vietnam Joint Project “Development of landslide risk assessment technology along the transport arteries in Vietnam”



tions: the Institute of Transport Science and Technology of Vietnam and the Forestry and Forest Products Research Institute of Japan, and the Japan Landslide Society. This application was accepted as one of a new joint programme by the MEXT and Ministry of Foreign Affairs of Japan to promote the scientific contribution of Japan to developing countries. A much larger budget than for Early Warning of Landslides, for 5–6 years, including an equipment donation budget and scholarship budgets will be allocated. The title is “Development of landslide risk assessment technology along transport arteries in Vietnam”. Figure 2.14 shows some examples of landslides along the National Highway No. 1 between Hue and Danang and also the Ho Chie Minh Route, which was expanded and paved as the second national highway connecting the Northern and the Southern areas of Vietnam after big landslide disasters in National Highway No. 1. Landslide risk assessment is a pressing issue for the development of Vietnam.

The joint research groups in Indonesia and China have developed new early warning equipment suitable for their countries inspired from their joint research and obtained 3 patents and 4 Intellectual property rights in their countries. The implementation of the joint research project has greatly boosted the research and fund raising capability for further research within the participating member countries.

## Bibliography

- Apip, Takara, K., Yamashiki, Y., Sassa, K., Ibrahim, A.B., Fukuoka, H. (2010). A distributed hydrological-geotechnical model using satellite-derived rainfall for shallow landslide warning in a large catchment. *Landslides*, Vol. 7, No. 3. 237–258.
- Liao, Z., Hong, Y., Wang, J., Fukuoka, H., Sassa, K., Karnawati, D., Fathani, F. (2010). Prototyping an experimental early warning system for rainfall-induced landslide in Indonesia using satellite remote sensing and geospatial datasets. *Landslides*, Vol. 7, No. 3, 317–324.
- Sassa K. (1988). Geotechnical model for the motion of landslides. *Proc. 5th International Symposium on Landslides*. “Landslides”, Balkema, 1: 37–56.
- Sassa, K. and Yin, Y. (2010). *Early Warning of Landslides*, Geological Publishing House. 166 pages. (13 papers submitted to the International Workshop on Early Warning of Landslide Disaster Risk Reduction in the Eastern Asian Region, 30 Nov.–5 December 2009 in Kunming, China).
- Sassa, K., Luciano Picarelli, L., Yin Y. (2008). Monitoring, prediction and early warning. *Landslides-Disaster risk reduction (the full color volume of Proc. the First World Landslide Forum)*, Springer, 351–375.
- Sassa, K., Nagai, O., Solidum, R., Yamazaki, Y., Ohta, H. (2010). An integrated model simulating the initiation and motion of earthquake & rain induced rapid landslides and its application to the 2006 Leyte landslide. *Landslides*, Vol. 7, No. 3, 219–236.
- Sassa, K., Yueping Y. (2010). *Early Warning of Landslides*. Geological Publishing House, 166 pages
- Uchimura, T., Towhata, I., Trinh Thi Lan Anh, Fukuda, J., Bautista, C.J.B., Wang, L., Seko, I., Uchida, T., Matsuoka, A., Ito, Y., Onda, Y., Iwagami, S., Kim, M-S.,

- Sakai, N. (2010). Simple monitoring method for precaution of landslides watching tilting and water contents on slopes surface. *Landslides*, Vol. 7, No. 3, 351–358.
- Yin, Y., Wang, H., Gao, Y., Li, X. (2010). Real-time monitoring and early warning of landslides at relocated Wushan town, the Three Gorge Reservoir, China. *Landslides*, Vol. 7, No. 3, 339–350.
- Yin, Y., Zheng, W., Liu, Y., Zhang, J., Li, X. (2010). Integration of GPS with InSAR to Monitoring and Early Warning of Landslides in Danba, Sichuan, China. *Landslides*, Vol. 7, No. 3, 359–366.



Landslides: Global Risk Preparedness

Sassa, K.; Rouhban, B.; Briceño, S.; McSaveney, M.; He, B. (Eds.)

2013, XVI, 387 p. 293 illus. in color., Hardcover

ISBN: 978-3-642-22086-9